Available online at www.sciencedirect.com
ScienceDirect
Experimental Eye Research 84 (2007) 529–536
EXPERIMENTAL EYE RESEARCH
www.elsevier.com/locate/yexer

New quantitative analysis, using high-resolution images, of oxygen-induced retinal neovascularization in mice

Yuichi Chikaraishi, Masamitsu Shimazawa, Hideaki Hara*

Department of Biofunctional Molecules, Gifu Pharmaceutical University, 5-6-1 Mitahora-higashi, 502-8585 Gifu, Japan

Received 29 June 2006; accepted in revised form 8 November 2006
Available online 17 January 2007

Abstract

Oxygen-induced retinopathy (OIR) has been widely studied as an animal model of retinal neovascularization diseases. Evaluation using this model is mainly performed by counting cell nuclei above the internal limiting membrane in serial cross-sections or by scoring in flat-mounted retinas. Quantitative evaluation is important for accurate elucidation of pathological conditions and the drug evaluations. We therefore attempted quantification using new imaging software and high-resolution images taken with a high-resolution CCD camera. Neonatal mice were exposed to 75% oxygen from postnatal day 7 (P7) to P12, then returned to room air until P17. At each evaluation time, mice were perfused with fluorescein-dextran, and flat-mounted retinas were prepared. Total images of the retinal vasculature were collected and analyzed using the imaging software. P17 normal retinas showed increases in computerized total tube area, total tube length, number of segments, and number of branch points (versus P7 normal retinas). These increases coincided with the development of the retinal vasculature between P7 and P17. P17 OIR retinas similarly showed increases in those parameters, and the number of nodes (thick regions exceeding the maximum width of the vessel) and the node area (abnormality induced by OIR) were markedly increased (versus P17 normal retinas). Accordingly, this approach is considered most suitable for evaluating the number of nodes and node area in this model. Quantification using the present imaging software should be useful for evaluating physiological and pathological neovascularizations in this OIR model.

Keywords: mice; neovascularization; oxygen-induced retinopathy; quantificational evaluation; retinal vasculature

1. Introduction

Retinal neovascular diseases, such as diabetic retinopathy and retinopathy of prematurity (ROP), are leading causes of irreversible failing vision and blindness. These diseases are assumed to involve pathological neovascularization within the vitreous, resulting from stimulation by excess production of those angiogenic growth factors (such as vascular endothelial growth factor; VEGF) associated with retinal ischemia (Aiello et al., 1995a, 1998). At present, no drug therapy is available for the prevention of retinal neovascularization, and indeed the only approved clinical treatment is laser photocoagulation, which ablates the ischemic retinal tissue and thereby suppresses the pathological neovascularization. However, this treatment may have adverse effects, including visual impairments such as loss of peripheral and night vision.

Oxygen-induced retinopathy (OIR) in the newborn animal has been widely used as an animal model of retinal neovascularization diseases (Madan and Penn, 2003). Various anti-angiogenic compounds such as VEGF-related molecules (Aiello et al., 1995b; Bainbridge et al., 2002; Eyetech Study Group, 2002), matrix metalloproteinase (MMP) inhibitors (Das et al., 1999; Garcia et al., 2002), steroids (Rotschild et al., 1999; Spandau et al., 2005), and NSAIDs (Nandgaonkar et al., 1999; Sharma et al., 2003; Wilkinson-Berka et al., 2003) have been evaluated using this model. Evaluation of the OIR model itself has been performed by two main methods. One is a qualitative method involving scoring in 12 equally sized

* Corresponding author. Tel./fax: +81 582 237 8596.
E-mail address: hidehara@gifu-pu.ac.jp (H. Hara).

0014-4835/$ - see front matter © 2006 Elsevier Ltd. All rights reserved.
doi:10.1016/j.exer.2006.11.007

sections (“clock hours”) in FITC-dextran-perfused or adenosine diphosphatase (ADPase)-stained retinas; scoring vaso-obliteration, capillary tufts and ridges; and counting neovascularization in clock hours in a manner similar to the clinical assessment of ROP (Higgins et al., 1999). The other is a quantitative method involving counting nucleic cells above the internal limiting membrane in serial cross-sections (Smith et al., 1994). Both the scoring and counting methods have disadvantages. The scoring evaluation covers the total retinal vasculature, and a large number of retinas can be scored in a fairly short time, but it is lacking in quantitative ability. On the other hand, although the counting evaluation is semi-quantitative, it is difficult to cover the total retinal vasculature and it is time-consuming. An other quantitative method is one that measures the neovascular tufts (Al-Shabrawey et al., 2005; Gardiner et al., 2005; Nagai et al., 2005). This method provides quantitative results and an indication that is close to the actual pathological neovascularization. However, this method is difficult to evaluate from an objective viewpoint.

To try to solve the above problems, computerized digital-image analyses of the retinal vasculature have been developed using retinopathy models (Penn and Gay, 1992; Danis and Yang, 1993; Reynaud and Dorey, 1994; Robison et al., 1995). The evaluated parameters were mostly retinal vascular density and area, and these methods allow an objective evaluation. However, no attempt has previously been made to evaluate pathological neovascularization (neovascular tufts), reflecting the clinical condition of retinopathy.

Therefore, the purpose of this study was to establish an objective and quantitative method that can be performed using imaging software on the whole retina in a mouse OIR model.

2. Materials and methods

2.1. Animals

C57BL/6 mice (SLC, Shizuoka, Japan) were used. All investigations were in accordance with the ARVO statement for the Use of Animals in Ophthalmic and Vision Research, and were approved and monitored by the Institutional Animal Care and Use Committee of Gifu Pharmaceutical University.

2.2. Oxygen-induced retinopathy model

The oxygen-induced retinopathy model was produced according to the protocol of Smith et al. (1994). Mouse pups and their nursing mothers were exposed to $75 \pm 1\%$ O_2 in a cage regulated by an oxygen controller (PRO-OX 110; Reming Bioinstruments Co., Redfield, USA) from postnatal day 7 (P7) to P12. The oxygen level was monitored using the oxygen controller. On P12, they were returned to room air (21% O_2) until P17.

2.3. Histological examination of retina

At P17, the eyes were removed, fixed in 4% paraformaldehyde in 0.1 M phosphate buffer for 24 h, and embedded in paraffin. Serial 6-μm sections of whole eyes were cut sagittally through the cornea parallel to the optic nerve. The sections were stained with hematoxylin and eosin to assess retinal vasculature via light microscopy.

2.4. Fluorescence angiography

At each evaluation time [P7, P12, and P17 (Fig. 1)], mice were deeply anesthetized intraperitoneally with sodium pentobarbital (Nembutal, Dainippon Sumitomo Pharmaceutical Co. Ltd., Osaka, Japan). Then, they were perfused through the left ventricle with high molecular weight (MW = 2,000,000) fluorescein conjugated dextran (Sigma–Aldrich Ltd., St. Louis, MO) dissolved in PBS. After the perfusion, the eyes were enucleated and placed in 4% paraformaldehyde for 4–24 h. The cornea and lens were removed from each eye. The posterior hyaloidal artery was removed from site connected with the optic nerve head by the forceps and the retinas were dissected under a microscope. The flattened retinas were mounted using VECTASHIELD (Vector Laboratories Inc, Burlingame, CA).

2.5. Quantification of retinal vasculature and scoring of retinal neovascularization

Total images of flat-mounted retina were produced from 9 to 12 pieces of images acquired using a fluorescence microscope (BX50; OLYMPUS, Japan) fitted with a ×4 microscope objective lens. Images were obtained using a high-resolution (2.6 μm^2/pixel, 16 bit) charge-coupled device (CCD) camera (DP30BP; OLYMPUS, Japan) at 1360×1024 pixels via Metamorph (Universal Imaging Corp., Downingtown, PA). Each piece of image was acquired from the stack images between upper and lower retinal vessels at 14.2-μm intervals, the best focus image being extracted from among them. The total images were converted from pixels to μm. Quantification of the retinal vasculature was achieved using Angiogenesis Application module in Metamorph. Minimum tubule width, maximal tubule width, and intensity were set up as setting items as described below. The minimum tubule width was taken as 1 μm. The maximal tubule width was obtained by measuring three times across one of the most dilated arteries or veins in each specimen, and taking the average of these measurements. The intensity was obtained by subtracting the intensity of the retinal background from the intensity of a faint vessel. The intensity of the retinal background was taken as the average of three minimum-intensity points. The intensity of a faint vessel was taken as the average of three points with neither minimum nor maximum intensity chosen from five points. We evaluated using six computed parameters: number of nodes, node area, total tube area, total tube length, number of branch points, and number of segments (as defined in Table 1). Retinal neovascularization scoring was performed using a method based on the scoring criteria (Table 2) described by Higgins et al. (1999). The scoring was performed by masked individuals to prevent observed bias.

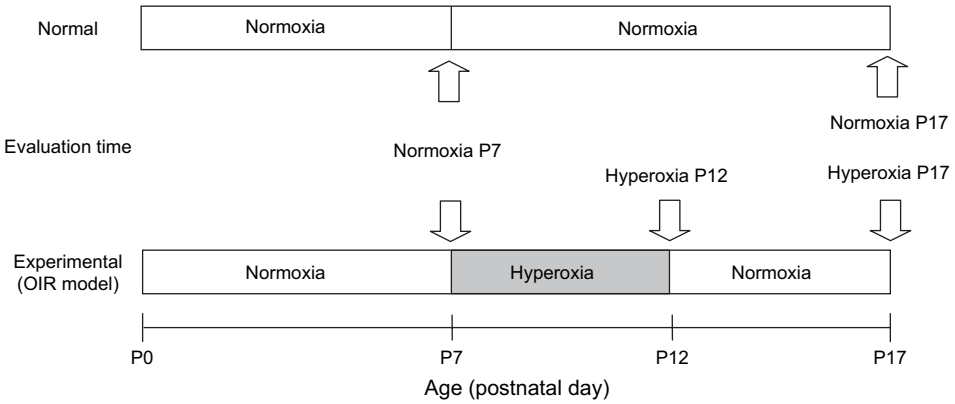

Fig. 1. Time course of study of retinal vasculature during normal development and oxygen-induced retinopathy in mice.

2.6. Statistical analysis

The data are represented as mean ± SEM. The Mann–Whitney test was used to compare P17 normal retinas with P17 OIR retinas. The correlation between either the number of nodes or the node area and the retinal neovascularization score was evaluated using the Pearson correlation coefficient. A value of $p < 0.05$ was considered to indicate statistical significance.

3. Results

3.1. Quantification of retinal vasculature

As in previous studies (Smith et al., 1994; Campochiaro and Hackett, 2003), the retinal vasculature in P7 neonatal mice was located in the superficial retina, and covered about 80% of the retina (Fig. 2A and E). Upon exposure of neonatal mice to 75% O_2 for 5 days (P7–P12), the retinal vessels around the optic nerve disappeared and an avascular area emerged (Fig. 2B and F). Following a return to room air until P17 after this hyperoxia treatment, P17 OIR retinas exhibited the following: revascularization forward avascular area, the appearance of tortuous and dilated blood vessels, and the appearance of abnormal vascular structures such as tufts and ridges (Fig. 2C and G). In contrast, the P17 normal retinal vasculature exhibited a meshwork in which development and remodeling were complete (Fig. 2D and H).

The P17 OIR retinal vasculature had obvious morphological differences versus the P17 normal retinal vasculature (Fig. 3A and B). This abnormal vasculature was located above the internal limiting membrane into vitreous (Fig. 3C and D). We quantitatively evaluated these sequential changes in the retinal vasculature using Angiogenesis Tube Formation in Metamorph. Original and analysis images are shown in Fig. 4. The retinal vessels seen in the analysis image for each group approximate to those in the original image (Fig. 4). Green labels in the analysis images represent nodes, one of the evaluation parameters. We evaluated six parameters obtained from these analysis images: total tube area, total tube length, number of branch points, number of nodes, node area, and number of segments (Fig. 5). The P17 normal retinas showed significant increases (1.8- to 2.6-fold) in total tube area, total tube length, number of segments, and number of branch points (versus P7 normal retinas) (Fig. 5C–F). The increases in these parameters coincided with the remodeling and development of the retinal vasculature between P7 and P17. The P17 OIR retinas similarly showed increases in the above four parameters, but the increases were apparently smaller than in the P17 normal retinas. Both the number of nodes and the node area in P17 OIR retinas showed marked increases (about fourfold) versus P17 normal retinas (Fig. 5A and B). In addition, the nodes region in the analysis images of the P17 OIR retinas corresponded well to the pathological neovascularization area (including tortuous and dilated blood vessels, and abnormal vascular structure) (Fig. 4G).

3.2. Quantification of vascular obliteration area

The central capillary-free zone occupied 36.0 ± 0.6% of the whole retina in P12 OIR retinas (just after hyperoxia), and 15.6 ± 0.7% in P17 OIR retinas.

Table 1
Definitions of measurements analyzed using Angiogenesis Tube Formation module in Metamorph

Measurement	Definition
Nodes	Total number of connected blobs (pooling of fluorescein conjugated dextran) with thickness exceeding maximum width of the vessels. Nodes region are shown as green in the acquired image
Nodes area	Total nodes area (mm^2) in retina
Total tube area	Total capillaries area (mm^2) in retina (excluding nodes)
Total tube length	Total length of capillaries (mm^2) in the retina (excluding nodes)
Branch points	Total number of junctions connecting segments (excluding nodes)
Segments	Total number of vessel segments connecting branch points and/or ends (excluding nodes)

Table 2
Retinal scoring criteria using flat-mounted retina

	0	1	2	3	4
Blood vessel growth	Complete	Incomplete outer third	Incomplete middle third	Incomplete inner third	–
Blood vessel tufts	None	Few, scattered (<3 h)	3–5 h	6–8 h	9–12 h
Extraretinal neovascularization	None	Mild (<3 h)	Moderate (3–6 h)	Severe (>6 h)	–
Central vasoconstriction	None	Mild, early zone 1 (inner 50% of zone 1)	Moderate (throughout zone 1)	Severe (extending to zone 2)	–
Retinal hemorrhage	Absent	Present	–	–	–
Blood vessel tortuosity	None	Mild (<3 h)	Moderate (3–6 h)	Severe (>6 h)	–

3.3. Retinal neovascular scoring and comparison with morphometric parameters

P17 normal ($n = 14$ eyes, open circle in Fig. 6) and OIR ($n = 12$ eyes, closed circle) retinas perfused with fluorescein-dextran were evaluated using retinal scoring criteria (Table 1). P17 OIR retinas had a median total retinopathy score [median (25th, 75th quartiles)] of 8.5 (7, 10) against 1 (0, 1) for the P17 normal retinas ($p < 0.001$). The Pearson's correlation coefficients between the nodes region parameters (number of nodes and node area) and the retinal neovascularization score are shown in Fig. 6. Both the number of nodes ($r = 0.95$, $p < 0.0001$) and the node area ($r = 0.85$, $p < 0.0001$) were highly correlated with the retinal neovascularization score. In the P17 OIR retina group alone, both the number of nodes ($r = 0.72$, $p = 0.008$) and the node area ($r = 0.79$, $p = 0.002$) correlated with retinal neovascularization score.

4. Discussion

Using an oxygen-induced retinopathy (OIR) model in mice, we analyzed the time course of changes in the retinal vasculature using high-resolution images of flat-mounted retinas and imaging software. Image analysis is a powerful tool for the assessment of retinal structure. Our study showed that the changes in microstructure occurring during the development of the retinal vasculature between P7 and P17 in normal retinas could be quantitatively evaluated as increases in each of several parameters (total tube area, total tube length, number of branch points, and number of segments). However, these parameters were also increased in the P17 OIR retina. On the other hand, the number of nodes and the node area increased significantly only in the P17 OIR retina, and showed little or no change in the other groups. Therefore, the present method, using imaging software, enables us to evaluate pathological changes in the vasculature by using the number

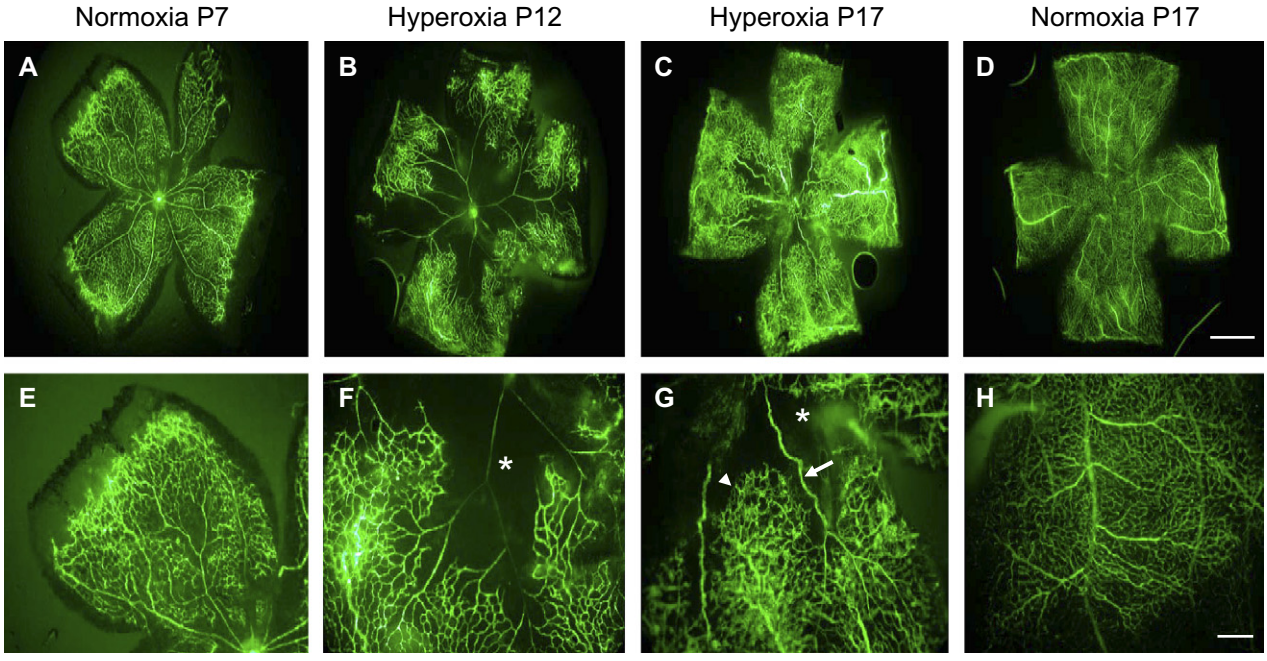

Fig. 2. Sequential changes in retinal vascularization in response to hyperoxia (fluorescein-dextran perfusion). Normal P7 retina before hyperoxia (A). At P7, superficial blood vessels cover about 80% of the retina (E). P12 retina, just after 5 days exposure to hyperoxia (B). Following exposure to hyperoxia, the region around the optic nerve has become an avascular area (asterisk) (F). Following return to room air after hyperoxia, the P17 retina exhibits tortuous and dilated blood vessels (arrow), loss of central vasculature (asterisk), and appearance of an abnormal vascular structure (arrowhead) (C and G). Normal P17 retina under room air (D). By P17, development and remodeling of retinal vasculature is complete (D and H). Scale bar in (D) = 1 mm and in (H) = 100 μm.

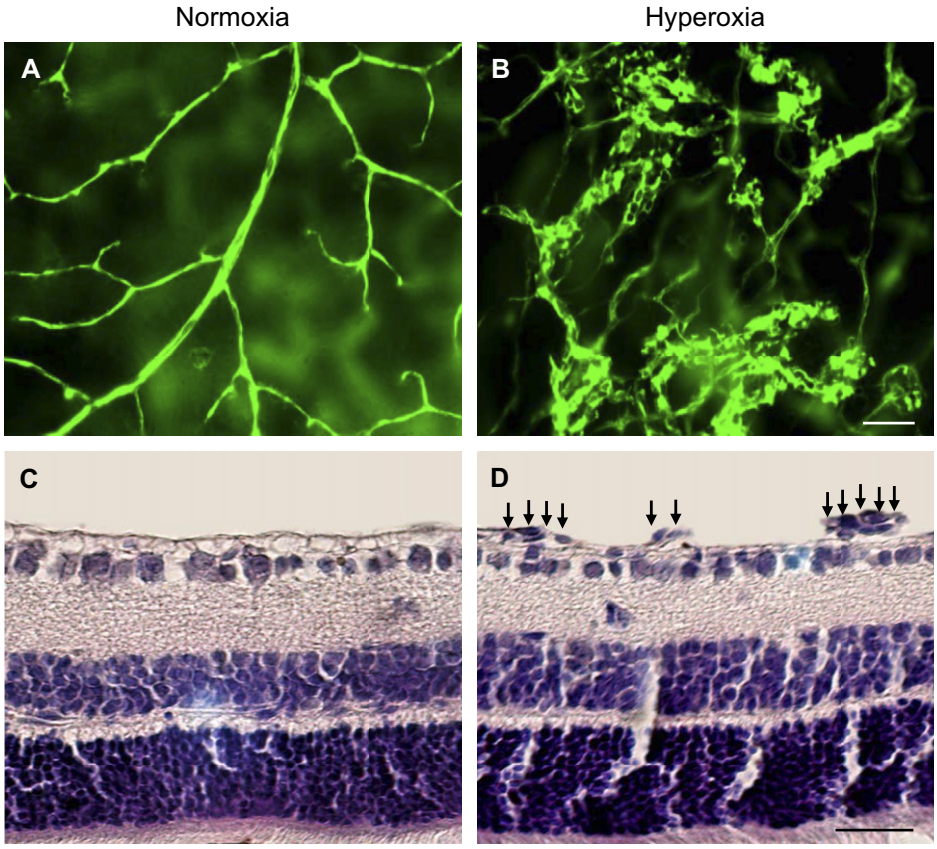

Fig. 3. Superficial retinal blood vessels on P17 retina. Normoxia- (A and C) and hyperoxia-treated (B and D) P17 retinas. Each fluorescence images (A and B) were collected from superficial retinal vasculature using a ×20 microscope objective lens. Following hyperoxia treatment, retinal vessels present a different pattern from normal. These neovascular tufts were confirmed by it extending into the vitreous (arrow) by cross-section images stained with hematoxylin and eosin (C and D). Scale bar is 50 μm for (A and B) and 25 μm for (C and D).

of nodes and the node area as indicators of abnormal neovascularization.

Some recent reports showed magnified figures of pathological neovascularization in flat-mounted retinas in this model (Al-Shabrawey et al., 2005; Gardiner et al., 2005). However, it is difficult, because of the lack of image resolution, to perform a detailed analysis in the whole retina. To solve this problem of lack of resolution, we obtained magnified figures of high-resolution images at 0.42 μm^2/pixel using a ×10 microscope objective lens and serial images at 2.7-μm intervals from the inner surface to the internal limiting membrane by scanning to the *z*-axis with a high-resolution CCD camera (DP30BP). These serial images were subsequently processed to create the best focus image, blurred region being eliminated by the imaging software. Using these images, abnormal neovascularization with aggregation and unregulated morphology extended beyond the internal limiting membrane into vitreous could be observed in P17 OIR retinas. Collectively, the present results indicate that the present method allows us to elucidate physiological and pathological neovascularizations, and would allow us to perform drug evaluations. Furthermore, the resolution of images in our analysis of the quantification of the retinal vasculature was 2.59 μm^2/pixel (using a ×4 microscope objective lens), sufficient to quantify vessels of about 7 μm minimum in the flat-mounted retina. Likewise, Banin et al. (2006) quantified physiological and pathological neovascularizations throughout the flat-mounted whole retina in a mouse OIR model, but the image resolution in their analysis was 27.8 μm^2/pixel (again, using a ×4 microscope − objective lens). This resolution may be insufficient for a detailed evaluation of microvessels of less than 25 μm.

Previously, evaluations using an OIR model in the newborn animal have mainly been performed either by scoring in clock hours in the flat-mounted retina (Higgins et al., 1999) or by counting nucleic cells above the internal limiting membrane in serial cross-sections (Smith et al., 1994). These evaluations have some problems involving lack of quantification or difficulty of covering the whole retina when quantitative information is obtained.

As one method of the quantitative evaluation using the flat-mounted retina, some investigators have reported measuring the tube area and length of retinal blood vessels using computer analyses (Penn and Gay, 1992; Danis and Yang, 1993; Robison et al., 1995; Al-Shabrawey et al., 2003; McGuire et al., 2003). However, simply evaluating tube area and length is insufficient to reflect the pathological changes of retinopathy that are evoked by cells invading into the vitreous. As another method, several studies have

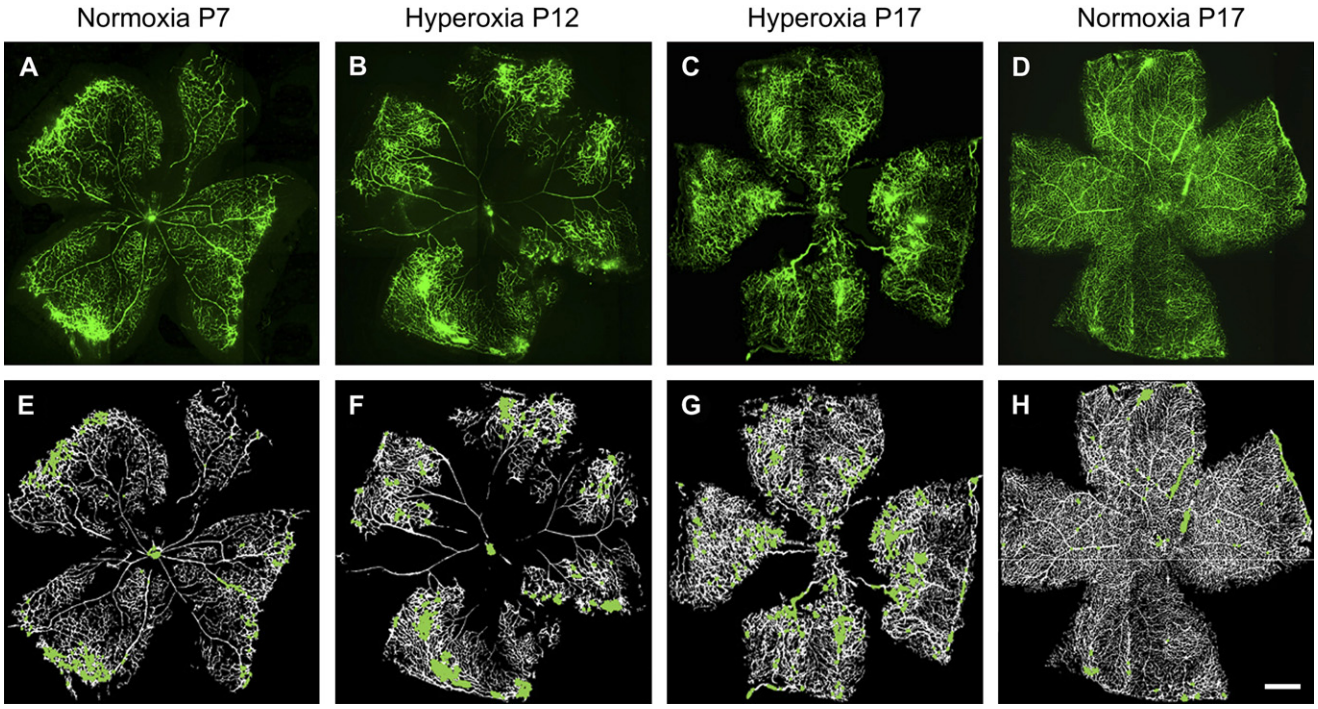

Fig. 4. Analysis images of retinal vascularization (obtained using Angiogenesis Tube Formation module). At various time-points [P7 normal before hyperoxia (nor-P7; A and E); P12 hyperoxia-treated (hyp-P12; B and F); P17 hyperoxia-treated (hyp-P17; C and G); and P17 normal (nor-P17; D and H)], mice were perfused with fluorescein-dextran, and flat-mounted retinas were prepared. Original images (A–D) and the analyzed images (E–H) are shown. Green labels in analyzed images show the node regions. Scale bar is 500 μm.

evaluated the pathological neovascularization (neovascular tufts) related to the symptoms of retinopathy (Al-Shabrawey et al., 2005; Gardiner et al., 2005; Nagai et al., 2005). This method entails observing the neovascular tufts under the microscope, selecting by hand, and calculating the selected area. However, it is difficult to exclude subjectivity, since the neovascular tufts are selected by hand. To try to avoid this problem, Banin et al. (2006) discriminated the above

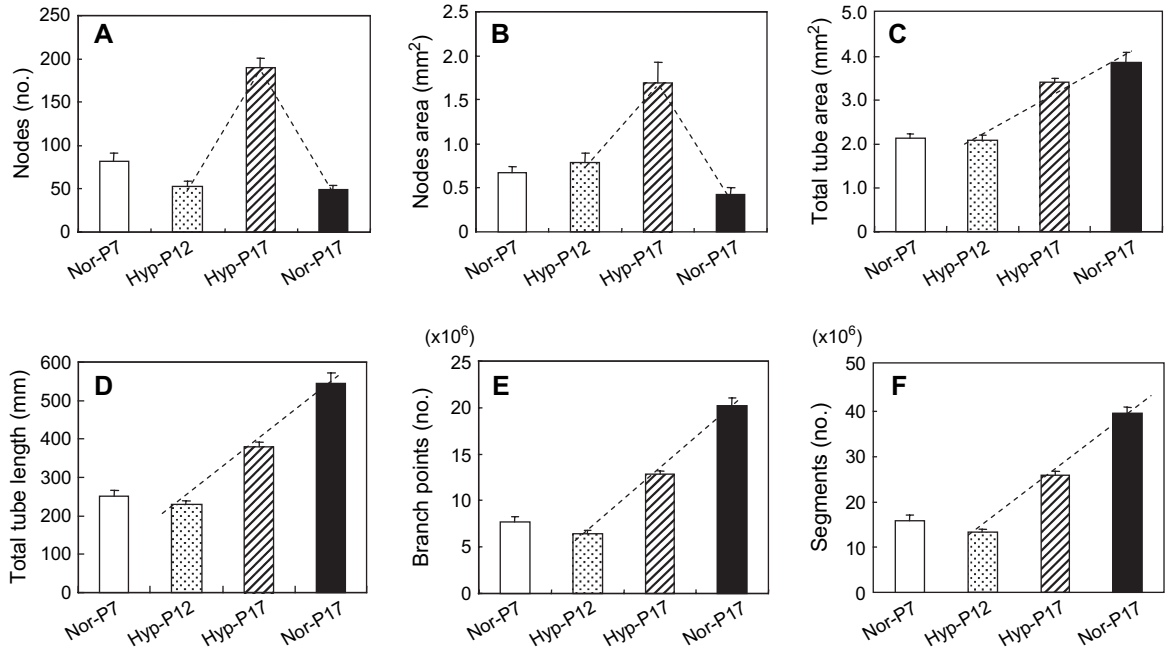

Fig. 5. Quantification of retinal vascularization using imaging software. Quantitative analysis of each parameter computed using Angiogenesis Tube Formation module: number of nodes (A), node area (B), total tube area (C), total tube length (D), number of branch points (E), and number of segments (F). Both the number of nodes (A) and the node area (B) were dramatically increased in the hyp-P17 group versus the nor-P17 group. The dotted line shows the time-dependent change. Values are means ± SEM; $n = 5–14$ eyes per group.

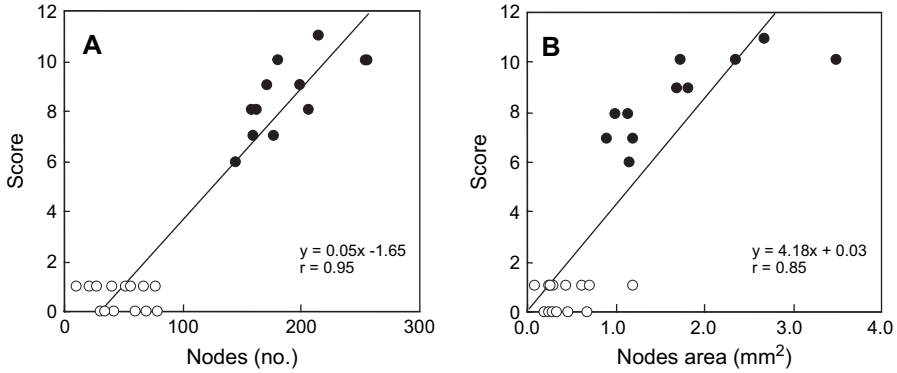

Fig. 6. Relationship between nodes (number and area) and retinal neovascularization score. Plots of number of nodes (A) and node area (B) against retinal neovascularization score for normal (open circle; $n = 14$ eyes) and hyperoxia-treated (closed circle; $n = 12$ eyes) retinal vasculatures at P17.

area by means of isolectin *Griffonia simplicifolia* staining, and then calculated the area. By immunostaining, the neovascular tufts can be distinguished specifically, and it is possible to exclude subjectivity if this area is delimited by threshold, in contrast to the previous method. However, since it is necessary to immunostain the retina, more time is required. As an evaluation method using an imaging software, Robison et al. (1995) reported a computerized evaluation using an indication similar to the number of nodes and node area employed in this report. Unfortunately, they evaluated only about 34% of the whole retina and required 35 image pieces for the analysis.

To overcome these defects, we attempted to computerize the retinal vasculature from the whole retinal image. Using our method, we could evaluate high-resolution images covering the whole retina, requiring 9–12 image pieces. Therefore, our method can save on evaluation time as compared with the previous methods. Furthermore, our results do not involve the bias introduced by subjective estimation, because of the computerized evaluation of the whole retina. In our scoring evaluation, both the number of nodes and the node area were highly correlated with the retinal neovascularization score. Since the scoring method needs a number of observers for reliability, our method, involving quantitative evaluation using imaging software, is more objective than the scoring method. As in a previous report (Banin et al., 2006), we observed revascularization, with a decrease in the avascular area, of the whole retina from P12 to P17 after hyperoxia. In addition, the size of the vascular obliteration area can be objectively evaluated, because the avascular borders are easily identified. Our method can objectively evaluate this revascularization in more detail using parameters such as total tube length, number of segments, and number of branch points. Furthermore, we could simultaneously evaluate how well anti-angiogenic drugs act against physiological and pathological angiogenesis.

In conclusion, the present new evaluation technique has several advantages: (1) the whole retina is covered using high-resolution images, (2) the physiological and pathological vasculature can be evaluated, and (3) the evaluations are quantitative. We therefore feel that it should be useful for the objective and quantitative evaluation of various agents in the mouse OIR model.

References

Aiello, L.P., Northrup, J.M., Keyt, B.A., Takagi, H., Iwamoto, M.A., 1995a. Hypoxic regulation of vascular endothelial growth factor in retinal cells. Arch. Ophthalmol. 113, 1538–1544.

Aiello, L.P., Pierce, E.A., Foley, E.D., Takagi, H., Chen, H., Riddle, L., Ferrara, N., King, G.L., Smith, L.E., 1995b. Suppression of retinal neovascularization in vivo by inhibition of vascular endothelial growth factor (VEGF) using soluble VEGF-receptor chimeric proteins. Proc. Natl. Acad. Sci. U.S.A. 92, 10457–10461.

Aiello, L.P., Gardner, T.W., King, G.L., Blankenship, G., Cavallerano, J.D., Klein, R., 1998. Diabetic retinopathy. Diabetes Care 21, 143–156.

Al-Shabrawey, M., El-Remessy, A., Gu, X., Brooks, S.S., Hamed, M.S., Huang, P., Caldwell, R.B., 2003. Normal vascular development in mice deficient in endothelial NO synthase: possible role of neuronal NO synthase. Mol. Vis. 9, 549–558.

Al-Shabrawey, M., Bartoli, M., El-Remessy, A.B., Platt, D.H., Matragoon, S., Behzadian, M.A., Caldwell, R.W., Caldwell, R.B., 2005. Inhibition of NAD(P)H oxidase activity blocks vascular endothelial growth factor overexpression and neovascularization during ischemic retinopathy. Am. J. Pathol. 167, 599–607.

Bainbridge, J.W., Mistry, A., De Alwis, M., Paleolog, E., Baker, A., Thrasher, A.J., Ali, R.R., 2002. Inhibition of retinal neovascularisation by gene transfer of soluble VEGF receptor sFlt-1. Gene. Ther. 9, 320–326.

Banin, E., Dorrell, M.I., Aguilar, E., Ritter, M.R., Aderman, C.M., Smith, A.C., Friedlander, J., Friedlander, M., 2006. T2-TrpRS inhibits preretinal neovascularization and enhances physiological vascular regrowth in OIR as assessed by a new method of quantification. Investig. Ophthalmol. Vis. Sci. 47, 2125–2134.

Campochiaro, P.A., Hackett, S.F., 2003. Ocular neovascularization: a valuable model system. Oncogene 22, 6537–6548.

Das, A., McLamore, A., Song, W., McGuire, P.G., 1999. Retinal neovascularization is suppressed with a matrix metalloproteinase inhibitor. Arch. Ophthalmol. 117, 498–503.

Danis, R.P., Yang, Y., 1993. Microvascular retinopathy in the Zucker diabetic fatty rat. Investig. Ophthalmol. Vis. Sci. 34, 2367–2371.

Eyetech Study Group, 2002. Preclinical and phase 1A clinical evaluation of an anti-VEGF pegylated aptamer (EYE001) for the treatment of exudative age-related macular degeneration. Retina 22, 143–152.

Garcia, C., Bartsch, D.U., Rivero, M.E., Hagedorn, M., McDermott, C.D., Bergeron-Lynn, G., Cheng, L., Appelt, K., Freeman, W.R., 2002. Efficacy of Prinomastat® (AG3340), a matrix metalloprotease inhibitor, in treatment of retinal neovascularization. Curr. Eye Res. 24, 33–38.

Gardiner, T.A., Gibson, D.S., de Gooyer, T.E., de la Cruz, V.F., McDonald, D.M., Stitt, A.W., 2005. Inhibition of tumor necrosis

factor-alpha improves physiological angiogenesis and reduces pathological neovascularization in ischemic retinopathy. Am. J. Pathol. 166, 637–644.

Higgins, R.D., Yu, K., Sanders, R.J., Nandgaonkar, B.N., Rotschild, T., Rifkin, D.B., 1999. Diltiazem reduces retinal neovascularization in a mouse model of oxygen induced retinopathy. Curr. Eye Res. 18, 20–27.

Madan, A., Penn, J.S., 2003. Animal models of oxygen-induced retinopathy. Front. Biosci. 8, 1030–1043.

McGuire, P.G., Jones, T.R., Talarico, N., Warren, E., Das, A., 2003. The urokinase/urokinase receptor system in retinal neovascularization: inhibition by A6 suggests a new therapeutic target. Investig. Ophthalmol. Vis. Sci. 44, 2736–2742.

Nagai, N., Noda, K., Urano, T., Kubota, Y., Shinoda, H., Koto, T., Shinoda, K., Inoue, M., Shiomi, T., Ikeda, E., Tsubota, K., Suda, T., Oike, Y., Ishida, S., 2005. Selective suppression of pathologic, but not physiologic, retinal neovascularization by blocking the angiotensin II type 1 receptor. Investig. Ophthalmol. Vis. Sci. 46, 1078–1084.

Nandgaonkar, B.N., Rotschild, T., Yu, K., Higgins, R.D., 1999. Indomethacin improves oxygen-induced retinopathy in the mouse. Pediatr. Res. 46, 184–188.

Penn, J.S., Gay, C.A., 1992. Computerized digital image analysis of retinal vessel density: application to normoxic and hyperoxic rearing of the newborn rat. Exp. Eye Res. 54, 329–336.

Robison, W.G., Laver, N.M., Jacot, J.L., Glover, J.P., 1995. Sorbinil prevention of diabetic-like retinopathy in the galactose-fed rat model. Investig. Ophthalmol. Vis. Sci. 36, 2368–2380.

Reynaud, X., Dorey, C.K., 1994. Extraretinal neovascularization induced by hypoxic episodes in the neonatal rat. Investig. Ophthalmol. Vis. Sci. 35, 3169–3177.

Rotschild, T., Nandgaonkar, B.N., Yu, K., Higgins, R.D., 1999. Dexamethasone reduces oxygen induced retinopathy in a mouse model. Pediatr. Res. 46, 94–100.

Sharma, J., Barr, S.M., Geng, Y., Yun, Y., Higgins, R.D., 2003. Ibuprofen improves oxygen-induced retinopathy in a mouse model. Curr. Eye Res. 27, 309–314.

Smith, L.E., Wesolowski, E., McLellan, A., Kostyk, S.K., D'Amato, R., Sullivan, R., D'Amore, P.A., 1994. Oxygen-induced retinopathy in the mouse. Investig. Ophthalmol. Vis. Sci. 35, 101–111.

Spandau, U.H., Sauder, G., Schubert, U., Hammes, H.P., Jonas, J.B., 2005. Effect of triamcinolone acetonide on proliferation of retinal endothelial cells in vitro and in vivo. Br. J. Ophthalmol. 89, 745–747.

Wilkinson-Berka, J.L., Alousis, N.S., Kelly, D.J., Gilbert, R.E., 2003. COX-2 inhibition and retinal angiogenesis in a mouse model of retinopathy of prematurity. Investig. Ophthalmol. Vis. Sci. 44, 974–979.